Hindawi
Shock and Vibration
Volume 2017, Article ID 3186584, 12 pages
https://doi.org/10.1155/2017/3186584

Research Article

Design, Modeling, and Analysis of a Novel Hydraulic Energy-Regenerative Shock Absorber for Vehicle Suspension

Junyi Zou,[1,2,3] Xuexun Guo,[1,2,3] Lin Xu,[1,2,3] Gangfeng Tan,[1,2,3] Chengcai Zhang,[1,2,3] and Jie Zhang[4]

[1] *School of Automotive Engineering, Wuhan University of Technology, Wuhan 430070, China*
[2] *Hubei Key Laboratory of Advanced Technology of Automotive Components, Wuhan University of Technology, Wuhan 430070, China*
[3] *Hubei Collaborative Innovation Center for Automotive Components Technology, Wuhan University of Technology, Wuhan 430070, China*
[4] *Technology Center, Wanxiang Group Corporation, Hangzhou 311215, China*

Correspondence should be addressed to Lin Xu; xulin508@whut.edu.cn

Received 13 February 2017; Revised 31 May 2017; Accepted 21 June 2017; Published 8 August 2017

Academic Editor: Carlo Trigona

To reduce energy consumption or improve energy efficiency, the regenerative devices recently have drawn the public's eyes. In this paper, a novel hydraulic energy-regenerative shock absorber (HERSA) is developed for vehicle suspension to regenerate the vibration energy which is dissipated by conventional viscous dampers into heat waste. At first, the schematic of HERSA is presented and a mathematic model is developed to describe the characteristic of HERSA. Then the parametric sensitivity analysis of the vibration energy is expounded, and the ranking of their influences is $k_1 \gg m_2 > m_1 > k_2 \approx c_s$. Besides, a parametric study of HERSA is adopted to research the influences of the key parameters on the characteristic of HERSA. Moreover, an optimization of HERSA is carried out to regenerate more power as far as possible without devitalizing the damping characteristic. To make the optimization results more close to the actual condition, the displacement data of the shock absorber in the road test is selected as the excitation in the optimization. The results show that the RMS of regenerated energy is up to 107.94 W under the actual excitation. Moreover it indicates that the HERSA can improve its performance through the damping control.

1. Introduction

With the energy consumption rising rapidly, the energy crisis is being more and more urgent. The proportion of transportation energy consumption increases year by year, and the percent of which will come up to 26%. In general, the transportation of people and goods accounts for about 25% of total world energy consumption. Passenger transportation, in particular, light-duty vehicles, accounts for most transportation energy consumption, with light-duty vehicles consuming more energy than all modes of freight transportation, including heavy trucks, marine, and rail combined [1]. So a great number of countries have initiated the development of renewable power. Among this, the vibration energy of vehicle is one of the sources that can be harvested. In Figure 1 [2], the vehicle energy flows of a 2.5 L 2005 Camry are demonstrated. And Figure 1 shows that most fuel energy is wasted. Therefore the energy regeneration can be considered as a new technology of energy saving, such as regenerative braking and regenerative suspension.

As to energy harvesting, it can be traced back to many years ago. Okada and Harada [3] demonstrated an electrodynamic regenerative damper, and the power was harvested by a linear motor in the system. Suda and Shiiba [4] designed a multiple suspension which could realize the active control and energy regeneration. The active control strategy of energy-regenerative shock absorber was improved. Roshani et al. [5] conducted an experimental program to evaluate the potential of harvesting energy from roadways using piezoelectric materials, and it showed that the quantity and arrangement of the piezoelectric sensors alter the applied stresses, which leaded to variations in the generated output power. Zuo et al. [6] developed an electromagnetic energy

harvester which could regenerate 16~64 W power at 0.25~0.5 m/s root mean square (RMS) suspension velocity. This study focused on the finite element method which carried out the analysis of magnetic field and optimization design. Li et al. [7] developed a shock absorber based on a permanent magnetic generator and a rack-pinion mechanism for energy harvesting and vibration damping. A peak power of 68 W and average power of 19 W could be attained at 48 km/h on a campus road. Singh and Satpute [8] designed an electromagnetic energy harvesting shock absorber, and a simulation with actual road excitation data indicated that the system could harvest 15 W of the average power from each wheel. Tang and Zuo [9] proposed a vibration energy harvester which composed of a spring-mass system. Comparison among the characteristics of dual-mass and single-mass was analyzed. The results also indicated that the harvesting power from vehicle suspension was proportional to tire stiffness and road vertical excitation spectrum. Montazeri-Gh and Soleymani [10] researched an energy storage system (ESS) in hybrid electric vehicles, and the simulation results revealed that the use of hybrid ESS could improve the efficiency of the batteries, and it could increase their working life as the active suspension (AS) load fluctuations were transferred from the batteries to the capacitors. Xie and Wang [11] proposed a dual-mass piezoelectric bar harvester which composed of a spring-mass system connected by a piezoelectric bar transducer which is equivalent to a spring and a damper in a mathematics model. And a power up to 738 W could be realized for a practical design of the harvester with a width and height of the piezoelectric bar of 0.015 m and 0.1 m, respectively. Wang et al. [12] designed a regenerative hydraulic shock absorber system which converted oscillatory motion of a vehicle suspension into unidirectional rotary motion of a generator. The power of 260 W and the efficiency of 40% were achieved by a shock absorber with piston rod dimensions of 50/30 mm under sinusoidal excitation of 1 Hz frequency and 25 mm amplitude when the accumulator capacity is set to 0.32 L with the load resistance 20 Ω. The appropriate damping characteristics could be realized by using variable load resistances and accumulator capacities. Guo et al. [13] developed an evaluation of energy harvesting shock absorbers on various vehicles, including passenger cars, buses, and trucks. An optimal analysis was developed to improve performance of ride comfort and road holding. Galluzzi et al. [14] applied a motion rectifier to improve energy recovery by constraining the motion of the electric motor to a single sense of rotation. This strategy can potentially reduce inertial issues related to zero-speed crossing and motion inversion; thus it could lead to the better conversion efficiency. Zuo and Zhang [15] investigated the performance of suspension with electromagnetic harvester. The tradeoff among energy harvesting, ride comfort, and road handling was analyzed. The study suggested that the road roughness, tire stiffness, and vehicle speed were greatly related to energy regenerating. 100~400 W average power was available at 60 mph on good and average roads. Fang et al. [16, 17] developed an electromagnetic shock absorber which could recover energy 200 W at the sinusoidal excitation of 10 Hz-3 mm. The energy harvesting efficiency decreased with the excitation frequency increase.

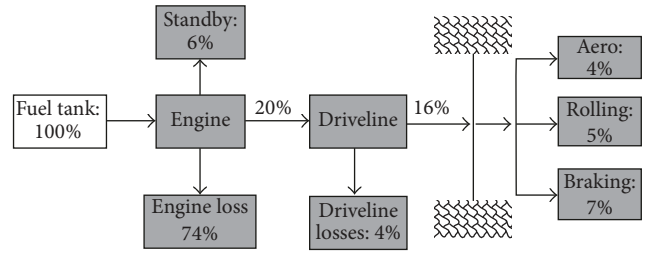

Figure 1: Vehicle energy flows of a 2.5 L 2005 Camry.

And an optimal algorithm was proposed to achieve active control and power maximization. Kammer and Olgac [18] conducted a concept study of a delayed-feedback vibration absorber to enhance energy harvesting, in which the delayed resonator theory was used for the energy harvesting purpose. Gong et al. [19] investigated the characteristic of a hydraulic-electricity energy-regenerative suspension. The optimization based on ride comfort and energy regeneration was obtained. Huang et al. [20] proposed a systematic methodology for predicting and optimizing the performance of an energy regeneration suspension system to efficiently capture the vibratory energy induced by the road irregularities. The method provided a graphic design guideline for the selection of stiffness and damping coefficients aimed at either best ride comfort or maximum energy harvesting.

The current article proposed a hydraulic electromagnetic shock absorber system. The modeling, analysis, simulation, and optimization of it are developed. And the analysis of the vibration energy is demonstrated to indicate that the potential of energy regeneration is immense. Thereafter, a parameter study and an optimization of HERSA are designed to improve the performance of it.

2. Schematic and Modeling of HERSA

2.1. System Configuration. The schematic of HERSA is described in Figure 1. The structure contains three components: a mechanical part which consists of a cylinder and a piston rod part; a hydraulic rectifier part which consists of accumulator, a hydraulic motor and pipelines; an energy-regenerative part which consists of a generator and a charging circuit including capacitances, inductances, and external loads. The piston in cylinder is distinguished from traditional shock absorber. The rebound valve and compression valve are removed, and only the by-pass valve and compensation valve are kept in the piston valve and bottom valve, respectively. In addition, the piston rod is hollow so that the fluid can flow to external parts.

As shown in Figure 2, the structure of HERSA is designed based on the conventional one. It has three tubes which include recovery tube, compression tube, and reservoir tube. However, in HERSA, the piston rod is hollow, so the fluid can flow through it to energy harvesting device. The rebound valve in piston and the compression valve in base valve system are wiped off. The hydraulic motor is connected with a generator via a shaft coupler. The energy-regenerative part

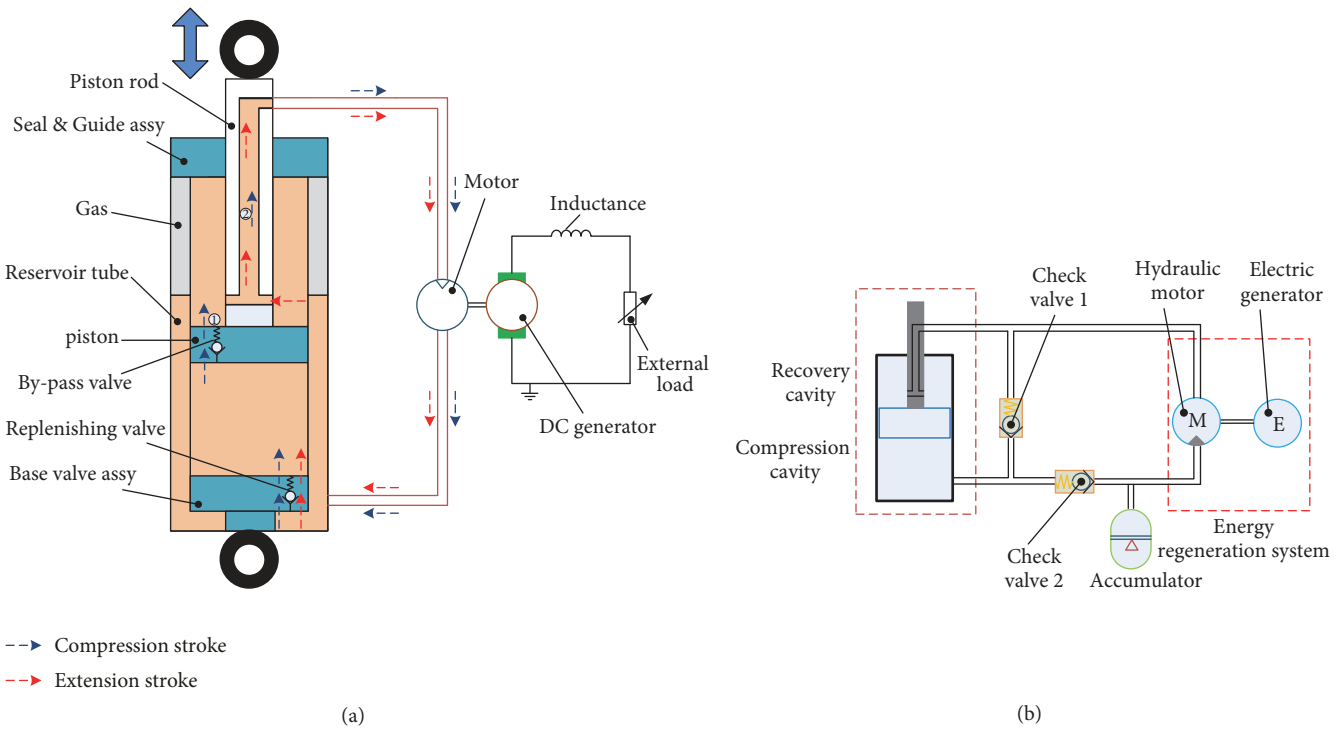

Figure 2: Schematic of HERSA. (a) The assembly diagram of HERSA. (b) The equivalent diagram of HERSA.

has a common rotating mechanism which can be founded in some references.

When in the extension stroke, the fluid flows from rebound chamber to hollow piston rod, then flows through the hollow channel in piston rod, along the pipeline to the hydraulic pump, flows through the hydraulic motor to the reservoir tube, and passes the replenishing valve back to the compression chamber at last. In this stroke, most energy can be harvested, and the external load can be adjusted to achieve semiactive suspension.

When in the compression stroke, the process is a little more complicated and the flow process can be divided into two parts:

(1) At first, because of the small cracking pressure, most of the fluid flows through the by-pass valve from compression chamber to replenishing chamber;

(2) After step (1), the upper chamber will be filled with oil. There is a volumetric difference between the upper and lower chamber because of the existence of piston rod. Just because of the volume difference, the residual oil in lower chamber will flow through the hollow piston to the regenerative part. As the volume of piston rod is small, so the volume of oil which flows into hydraulic motor is small too, and finally the harvested energy is little.

2.2. Mathematic Model of HERSA. Based on the working principle of HERSA shown in the Figure 2, a mathematic model is proposed to demonstrate the system dynamics, such as the damping characteristic. In the system, the hydraulic flow and generator circuit are important to the characteristic.

In the shock absorber, the damping force can be defined below:

$$F_c = P_f S_f - P_y S_y, \tag{1}$$

where P_f and P_y are, respectively, pressure of upper and inferior chamber and S_f and S_y are the ring area and surface area of piston.

While taking into account internal leakage in the system, it is understood that the fluid should flow through the check valve, the pipeline, and the hydraulic motor-generator circuit. The damping force is dependent on the three parts above. To describe the damping characteristic in detail, the two aspects, the hydraulic and the circuit system, are described, respectively.

2.2.1. Modeling of the Hydraulic System. In the extension stroke, the fluid firstly flows through the elbow in the hollow piston rod. This elbow can lead to the pressure partial loss, so the pressure drop can be presented by

$$\Delta P_{jc} = \frac{\varepsilon \rho v_{jc}}{2}, \tag{2}$$

where ΔP_{jc} is the pressure drop of elbows in the hydraulic system; ε is the local resistance coefficient; ρ is the density of hydraulic oil; v_{jc} is the flow velocity of the oil in this area.

Then the fluid flows through the hollow piston rod; the hollow channel can be simplified as a pipeline of short length.

Assuming the fluid is in laminar flow state, so the pressure drop can be presented by

$$\Delta P_l = \lambda \rho \frac{l_l v_l^2}{2}. \tag{3}$$

In the rubber hose, there are the common equations

$$\lambda = \frac{80}{R_e} \tag{4}$$

$$R_e = \frac{2 r_l v_l}{u_v}. \tag{5}$$

Combining (4) with (5), (3) can be presented by

$$\Delta P_l = \frac{10 u_v \rho l_l v_l}{{r_l}^2}, \tag{6}$$

where ΔP_l is the pressure drop in pipeline; λ is the coefficient of tube friction; l_l is the length of pipeline; v_l is the flow velocity of oil; r_l is the radius of pipeline; R_e is the Reynolds number; u_v is the kinematic viscosity of oil.

The valves in piston valve or base valve can lead to flow pressure drop; the check valves above are regarded as thin-wall holes, so the pressure drop can be presented by

$$Q_i = C_d S_i \sqrt{\frac{2 \Delta P_i}{\rho}} \tag{7}$$

$$\Delta P_i = \frac{{Q_i}^2 \rho}{2 C_d {S_i}^2}, \tag{8}$$

where ΔP_i is the pressure drop of the check valve i; Q_i is the flow rate of the check valve i; C_d is the flow coefficient; S_i is the cross area of the check valve i.

The reservoir tube in Figure 1 can be treated as an accumulator in the system; the gas is assumed to be ideal gas. According to Boyle's law, the gas pressure can be presented by

$$\begin{aligned} P_0 {V_0}^n &= P_g {V_g}^n \\ P_g &= P_0 \left[\frac{V_0}{V_0 - \left(S_y - S_f \right) \int v(t)\, dt} \right]^n, \end{aligned} \tag{9}$$

where P_0 is the initial charge pressure of gas in reservoir tube; V_0 is the initial charge volume; P_g and V_g are, respectively, the gas pressure and volume after the fluid flows into reservoir tube; n is the gas polytropic index; $v(t)$ is the velocity of piston.

2.2.2. Modeling of the Hydraulic System. The electric circuit consists of a motor, a DC generator, and an energy recovery circuit, where the circuit includes the inductances and the external resistances.

In the extension stroke, the high pressure oil drives the hydraulic motor; then the motor drives the generator by a coupler. According to their connection, the rotational speed and the output torque of hydraulic motor can be presented by

$$\begin{aligned} n_{\mathrm{hm}} &= \frac{Q_{\mathrm{hm}}}{q} \eta_v \\ T_{\mathrm{hm}} &= \frac{\Delta P_m q}{2\pi} \eta_m, \end{aligned} \tag{10}$$

where n_{hm} and T_{hm} are, respectively, the rotational speed and output torque of the hydraulic motor; q is the motor displacement; Q_{hm} is the flow rate through the hydraulic motor; ΔP_m is the pressure drop between the inlet and outlet of hydraulic motor; η_v and η_m are, respectively, the volumetric efficiency and mechanical efficiency of the hydraulic motor.

The hydraulic motor drives the generator. According to the moment equilibrium principle and the law of electromagnetic induction, the electromotive force (EMF) voltage, the electromagnetic torque, and the input torque of generator can be presented by

$$\begin{aligned} T_{Gi} &= J_m \dot{\omega} + T_e \\ T_e &= k_t I \\ U_e &= k_v \omega = IR, \end{aligned} \tag{11}$$

where T_{Gi} is the input torque of generator; J_m is the total rotational inertia of motor-generator unit; ω is the rotational speed of generator; T_e is the electromagnetic torque of generator in power regenerated status; k_t and k_v are the torque constant and EMF constant of generator, respectively; U_e is the EMF voltage; I is the electric current in the circuit; R is the resistance in the circuit.

Ignoring the rotational inertia of the rotor in generator [21], the pressure drop of hydraulic motor can be presented by

$$\Delta P_m = \frac{4\pi^2 Q_{\mathrm{hm}} k_t k_v \eta_v}{q^2 R \eta_m}. \tag{12}$$

As to the compression stroke, the volumetric difference can lead to fluids flow through the hydraulic motor, so the pressure drop can be presented by

$$\Delta P_{vm} = \frac{4\pi^2 Q_{vm} k_t k_v \eta_v}{q^2 R \eta_m} \tag{13}$$

$$Q_{vm} = S_v |v| = \pi {r_v}^2 |v|, \tag{14}$$

where ΔP_{vm} is the pressure drop of the hydraulic motor in compression stroke; Q_{vm} is the flow rate through the hydraulic motor; S_v is the cross area of the hollow piston rod wall; r_v is the equivalent radius of the cross area.

Ignoring the internal leakage in hydraulic cylinder, the flow rate in all parts of the hydraulic system is the same, so it can be presented by

$$Q_c = S_f |v| = S_i v_i = \pi {r_l}^2 v_l = \pi {r_l}^2 v_{jc}. \tag{15}$$

According to the pressure equation, the pressure in the system can be presented by

$$P_f = P_y + \Delta P_{jc} + \Delta P_l + \Delta P_i + \Delta P_m. \tag{16}$$

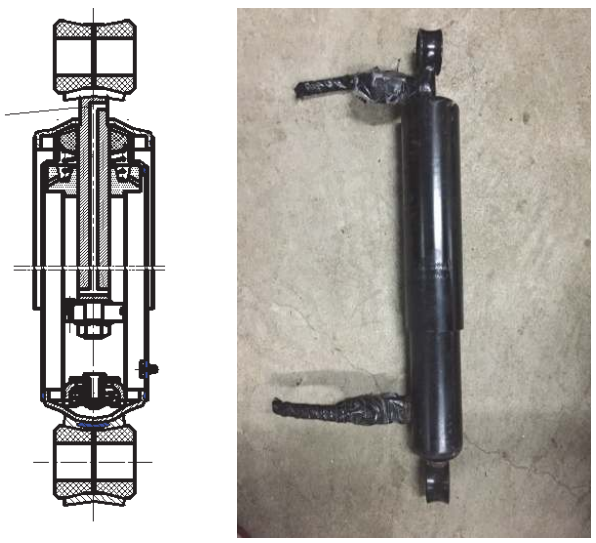

(a) (b)

Figure 3: The prototype of the cylinder. (a) The drawing of the cylinder. (b) The fabrication of the cylinder.

Therefore, based on the above inference, the damping force can be presented by

$$\begin{aligned} F_{cy} &= P_g\left(S_y - S_f\right) + \frac{\rho {S_y}^3 v(t)^2}{2C_d {S_2}^2} + \frac{4\pi^2 Q_{vm} k_t k_v}{q^2 R \eta_m} \\ &\quad + \frac{10 u_v \rho l_l {S_y}^2}{\pi {r_l}^4} v(t) + \frac{\varepsilon \rho {S_y}^3}{2\pi^2 {r_l}^4} v(t)^2 \\ F_{ce} &= P_g\left(S_f - S_y\right) + \frac{\rho {S_y}^3 v(t)^2}{2C_d {S_1}^2} + \frac{4\pi^2 Q_{\mathrm{hm}} k_t k_v}{q^2 R \eta_m} \\ &\quad + \frac{10 u_v \rho l_l S_y S_f}{\pi {r_l}^4} v(t) + \sum \frac{\varepsilon \rho S_y {S_f}^2}{2\pi {r_l}^4} v(t)^2 . \end{aligned} \tag{17}$$

In the equation, F_{cy} and F_{ce} are the damping force in compression stroke and extension stroke, respectively.

2.3. Prototype of the Cylinder in HERSA. As shown in Figure 3, the prototype of the cylinder in HERSA is fabricated on the basis of a traditional shock absorber according to the conceptual design in Figure 2. In consideration of the worse road excitation of SUVs or heavy trucks, this design target is commercial vehicle. The primary components in the system are a hydraulic cylinder, a motor, oil tubes, and a DC generator.

3. Analysis of Suspension Vibration Energy

3.1. Suspension Vibration Energy. The road roughness can lead to the vibration of the vehicle suspension. The vibration energy is transformed into thermal energy by the traditional shock absorber. To analyze the vibration energy, the suspension vibration equation is given in Figure 4.

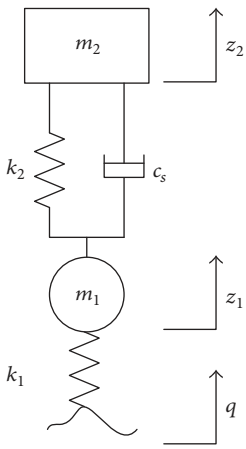

Figure 4: Dynamic model of 2-DOF suspension.

$$\begin{aligned} &m_2 \ddot{z}_2 + c_s\left(\dot{z}_2 - \dot{z}_1\right) + k_2\left(z_2 - z_1\right) = 0 \\ &m_1 \ddot{z}_1 + c_s\left(\dot{z}_1 - \dot{z}_2\right) + k_2\left(z_1 - z_2\right) + k_1\left(z_1 - q_{\mathrm{road}}\right) \\ &\quad = 0, \end{aligned} \tag{18}$$

where m_2 and m_1 are, respectively, the sprung and unsprung mass; $\ddot{z}_2$ and $\ddot{z}_1$ are, respectively, the acceleration of sprung and unsprung mass; k_2 and k_1 are, respectively, the stiffness of spring and tire; q_{road} is the road roughness.

The instantaneous dissipation power of suspension can be presented by

$$\begin{aligned} P_s &= c_s\left(\dot{z}_2 - \dot{z}_1\right)^2 \\ P_t &= \int_T P_s(t)\, d(t), \end{aligned} \tag{19}$$

where P_s is the dissipation power of suspension; c_s is the damping coefficient of the system; $\dot{z}_2$ and $\dot{z}_1$ are, respectively, the velocity of sprung mass and unsprung mass; T is the vibration period of suspension; $P_s(t)$ is the dissipation power of suspension at t moment.

The vibration energy is transformed into thermal energy in conventional suspension. But in the HERSA, the special structure determines the vibration power conversion; one part is converted into heat energy and the other part is converted into electric energy which can be regenerated. For the HERSA system, the power flow can be demonstrated in Figure 5.

As shown in Figure 5, the vibration energy includes two parts: thermal P_{th} and electric P_{el} power; the thermal power P_{th} consists of the mechanical friction power P_{m1}, the check valve damping power P_c, the pipeline and elbow damping power P_p, the power stored in reservoir tube P_r, the mechanical and volumetric power dissipated in motor-generator P_{m2}, and power dissipated on internal resistance P_{rin}. The power flow equation can be presented by

$$P_t = P_{\mathrm{th}} + P_{\mathrm{el}} = P_{m1} + P_c + P_p + P_r + P_{m2} + P_{\mathrm{rin}} + P_{\mathrm{el}}. \tag{20}$$

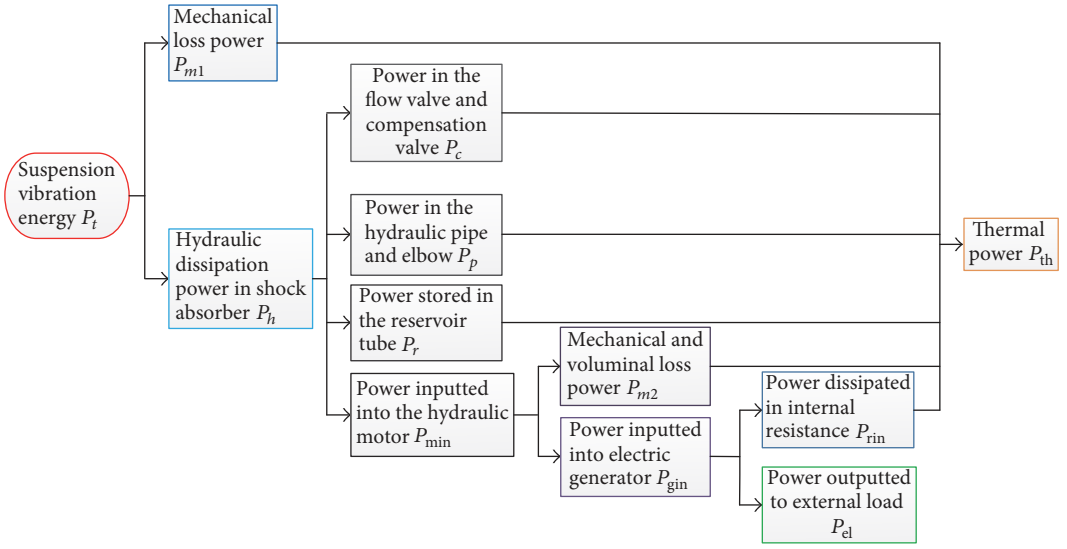

Figure 5: Power flow chart of suspension vibration energy.

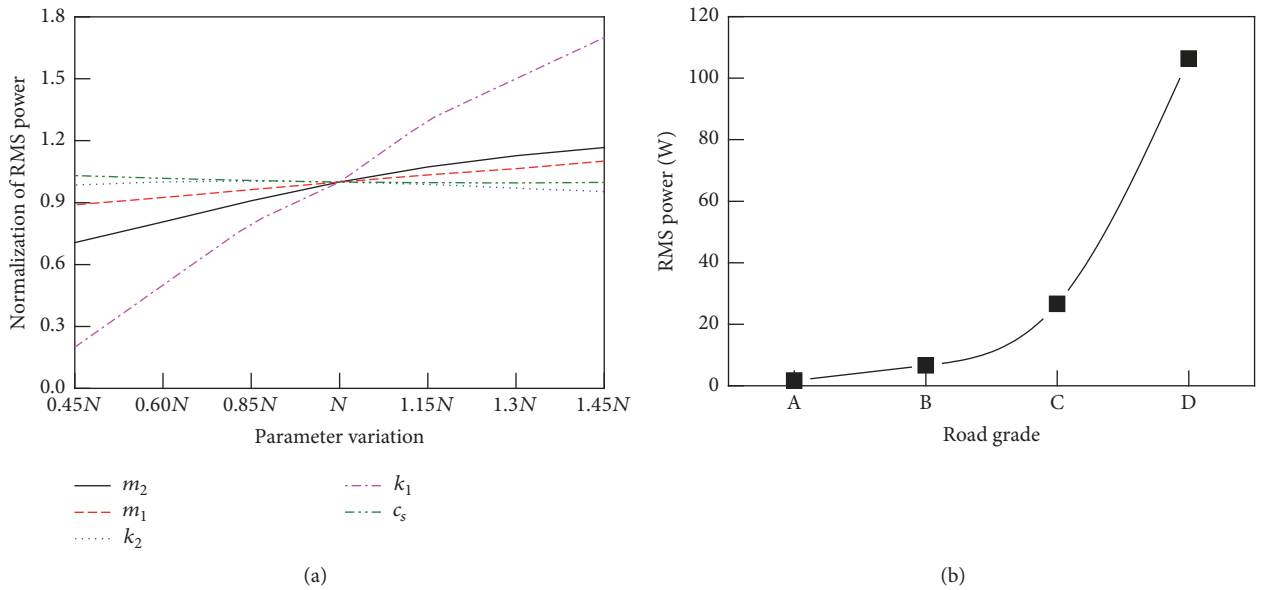

Figure 6: Parameter analysis of suspension vibration energy. (a) The influence of the parameters on RMS dissipation power, on the B grade road. (b) The influence of different roads on RMS dissipation power.

3.2. Sensitivity Analysis of Suspension Vibration Energy. The vibration energy is related to suspension system and the road, so the parameter study is carried out to analyze the sensitivity. A model of quarter vehicle is established to analyze the influences of vehicle parameters on vibration energy. The values of the parameters are demonstrated in Table 1.

Based on the parameters in the Table 1, a simulation model is carried out to evaluate the influences of the vehicle parameters and different grade roads on suspension vibration energy.

In Figure 6(a), one parameter changes while the others are kept at nominal value. The N represents the nominal value of the parameters, and the parameters change in same proportion of $0.15N$. The influences of the parameters on vibration energy are as follows:

Table 1: Parameters of the quarter vehicle model.

Parameter of vehicle	Valve
Sprung mass/m_2	350/kg
Unsprung mass/m_1	40/kg
Spring stiffness/k_2	20000/(N·m^{-1})
Tire stiffness/k_1	180000/(N·m^{-1})
Damping rate/c_s	1500/(N·s·m^{-1})

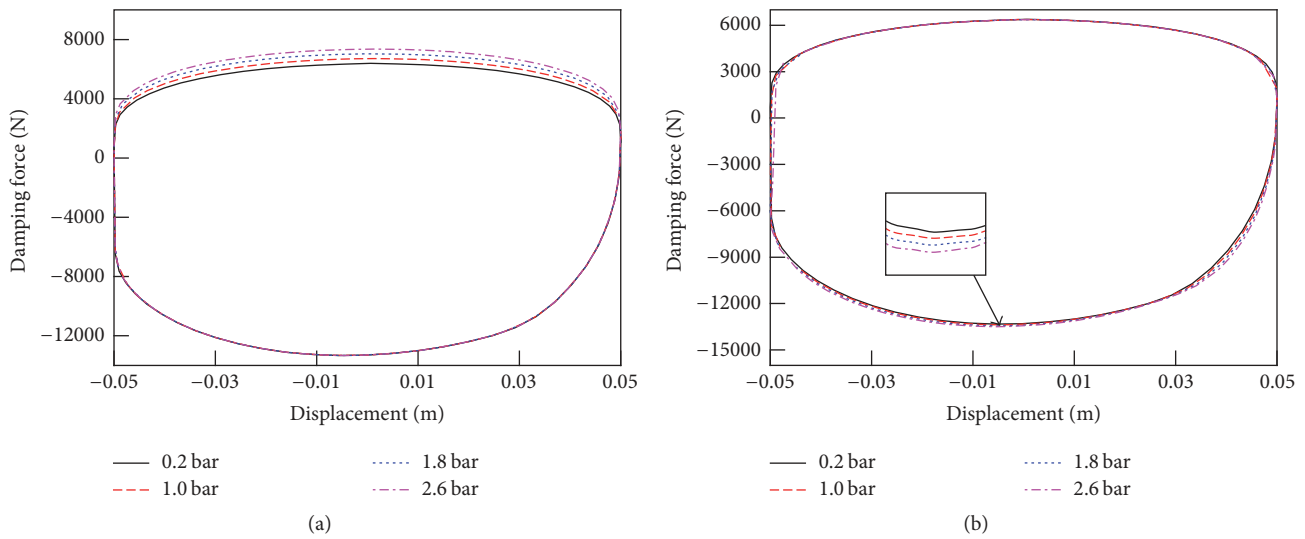

Figure 7: The influence of check valve in HERSA. (a) The influence of by-pass valve on damping characteristics. (b) The influence of replenishing valve on damping characteristics.

(1) The RMS power is proportional to k_1, m_2, and m_1, and the increasing rate ranking is $k_1 \gg m_2 > m_1$;

(2) The k_2 and c_s almost have no influences on vibration energy, and the RMS power decreases at first and gradually tends to a constant value as c_s increases;

(3) In Figure 6(b), the road grade is according to the ISO standard [21]. The RMS power increases with the road grade increases from A to D, and the increasing rate gets bigger and bigger from A to D. The results are coincident with the results in Galluzzi et al. [14].

4. Parametric Analysis of HERSA

In the HERSA, there are many components in the system, such as the hydraulic cylinder, the piston, the pipeline, the check valve, the reservoir tube, the motor, the generator, and the electric elements. The parameter is enormous. The initial parameter valve of HERSA is shown in Table 2.

In this paper, the parameters are various and shown in Table 2; the effects of them on the damping characteristics of HERSA and regenerated energy are demonstrated in the following analysis. A sinusoidal excitation is set as the road roughness, and it can be presented by

$$q_{\text{road}} = A \sin(2\pi f t). \tag{21}$$

A and f are, respectively, the amplitude and frequency of the sinusoidal excitation, and the initial valves of A and f are 50 mm and 1.67 Hz respectively.

4.1. Parameter Study

4.1.1. Check Valve. In the system, there are by-pass valve and replenishing valve. The by-pass valve mainly works in the compression stroke, and the replenishing valve mainly works in the extension stroke. And the key parameter of valves is the cracking pressure. It affects greatly the damping force, and the influence diagram is presented in Figure 7.

Table 2: Parameters of the HERSA.

Parameter	Valve
D	65 mm
d	26 mm
ρ	850 (kg/m^3)
P_0	15 bar
V_0	0.5 L
q	10 (mL/r)
η_v	0.9
n	1.2
J_m	10^{-7} (kg·m^2)
$P_{\text{crack-valve 1}}$	0.2 bar
l_l	500 mm
r_l	25 mm
c_d	0.6
k_t	0.25 (N·m/A)
k_v	0.25 (V·s/rad)
ε	1.34
η_m	0.9
R_{in}	0.6 Ω
R_{ou}	15 Ω
$P_{\text{crack-valve 2}}$	0.2 bar

As shown in Figure 7, the by-pass valve works in the compression stroke, so, in Figure 7(a), the damping force in extension stroke almost has no changes, whereas the damping force in compression stroke increases with the increase of cracking pressure. For the by-pass valve, the increase of ΔP leads to the damping force increasing according to (8). As to Figure 7(b), the damping force in the extension stroke

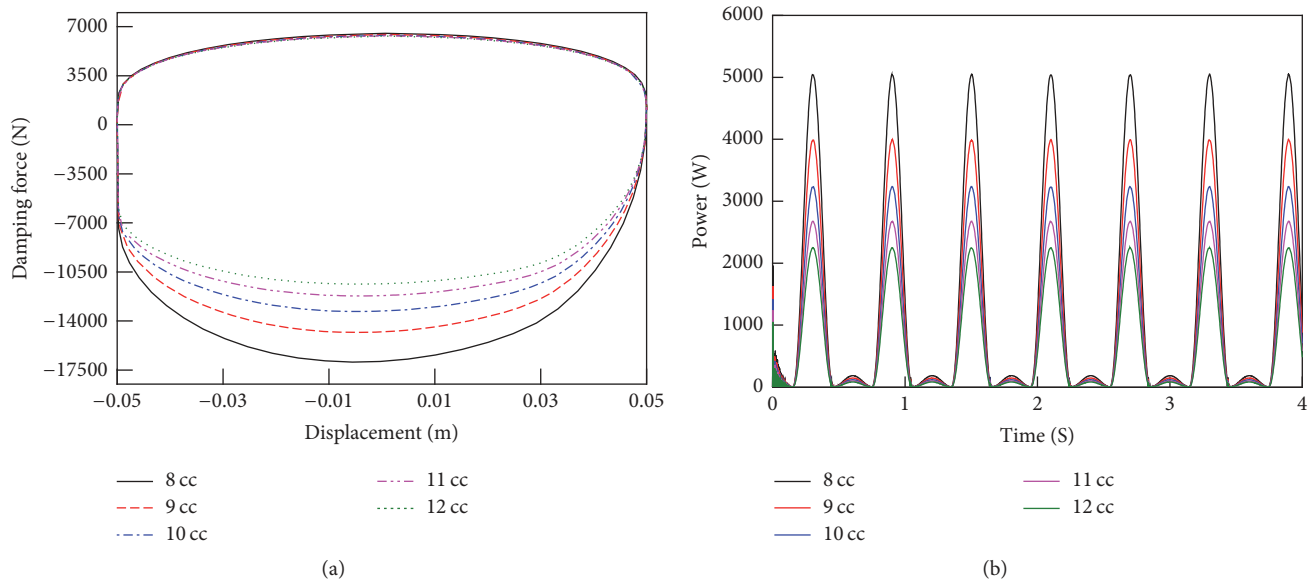

Figure 8: The influence of hydraulic motor on HERSA. (a) The indicator diagram of HERSA. (b) The influence on energy-regenerative characteristics.

increases with the increase of cracking pressure, and the influence is tiny.

4.1.2. Hydraulic Motor. The hydraulic motor is the energy conversion part, and the vibration energy is put into the DC generator to generate electricity, in which the displacement of motor plays an important role in the influence on the flow characteristic of the fluid, which results in the change of pressure difference between import and export in motor. Damping and energy-regenerative characteristic can change with it.

It can be seen from Figure 8 that the motor hydraulic displacement has a negative correlation with damping force in extension stroke and regenerative power. In Figure 8(a), the influence of motor displacement on rebound force is unobvious. The motor speed decreases with motor displacement increases. The pressure drop in motor decreases too. So the damping force decreases according to (12). The motor with high speed can drive the generator to revolve faster and acquires more power.

4.1.3. The External Load R_{ou}. The external load is a significant element for the damping force and the regenerative power. The indicator diagram and the regenerative power under different external loads are demonstrated in Figure 9, respectively.

The influences of the external load on the characteristic of HERSA are shown in Figure 9. According to (12), the pressure drop of the hydraulic motor decreases with the external load increases. So in Figure 9(a), the damping force of extension decreases with the increase of external load; and in Figure 9(b), the peak regenerative power in the extension stroke decreases with the increase of external load.

When HERSA is in compression stroke, the volumetric difference can lead to fluids flow through the hydraulic motor. But the amount of the fluids is very small because the wall thickness of piston rod is small. According to (13), the small Q_{vm} can cause tiny influence on the damping force. So the influence in extension stroke is put forward in the Figure 9.

5. Optimization of HERSA

For the HERSA, the design goal is to regenerate more power as far as possible without devitalizing the damping characteristic. In order to achieve this goal, an optimization is carried out to get the optimal q and R_{ou}. In the optimization, there is one object and two constraints, whose object is the maximum of the RMS power. The procedure diagram of optimization is shown in Figure 10.

As shown in Figure 10, the first step is to determine the design variables, which include motor displacement and external load. The reason is that such two parameters have great influences on damping and energy-regenerative characteristics as shown in Section 4. Moreover, the external load is a controllable variable for the semiactive control of suspension. So the design variables and constraint are shown in the Table 3.

5.1. Vibration Input. In Sections 3 and 4, the simulation is based on the test standard of shock absorber, so the excitations should be sinusoidal excitation. But in practical road condition, the pavements are random. The sinusoidal excitation cannot demonstrate the real excitation input. In this paper, to make the optimization more close to the practical condition, the excitation input of shock absorber is collected through a road test.

As shown in Figure 11(a), the chosen vehicle in the test is a heavy truck which conforms to the design requirements. The reason is that the road conditions of commercial vehicles such as SUV and trucks are worse than which of ordinary

Table 3: Parameter determination of the optimization.

Parameter determination		Range
Variable determination	Hydraulic motor displacement/Dis	5~40/(mL/r)
	External load/R	5–40/Ω
Constraint condition	F_{ce}	8000~12000/(N)
	F_{cy}	−6000~−3000/(N)

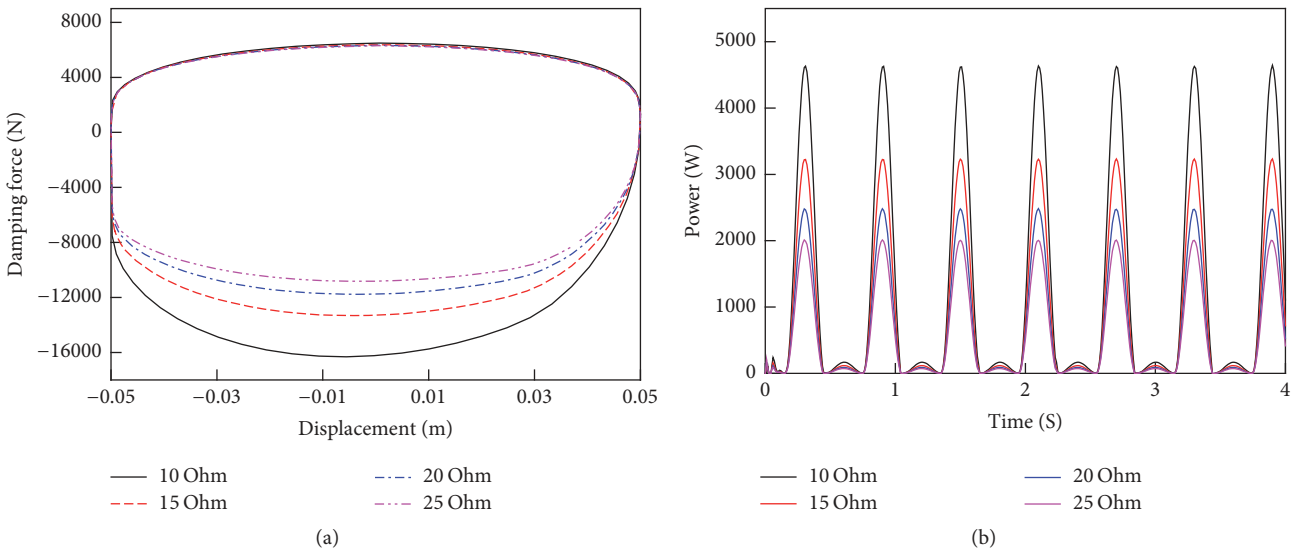

Figure 9: The influence of external load on HERSA. (a) The indicator diagram of HERSA. (b) The influence on energy-regenerative characteristics.

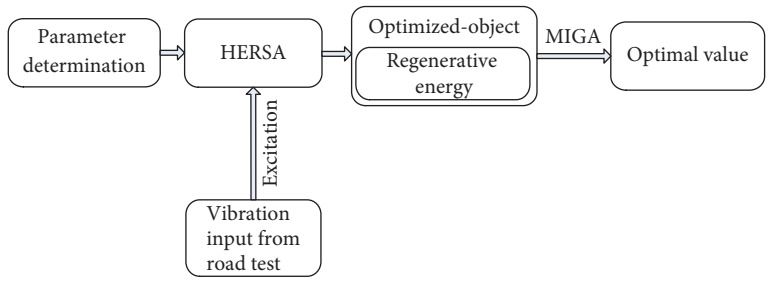

Figure 10: The optimization procedure diagram.

passenger cars, and according to the relative analysis in Section 3, the commercial vehicles on worse road have bigger energy-regenerative potential. So a light truck is selected for this test. Figures 11(c) and 11(d) are displacement sensor and data collection equipment, respectively. The suspension working states can be obtained through the test above.

To analyze the effects of different parameters on HERSA, several special road pavements are selected to compare the performance of HERSA. And Figure 12 is physical image of these roads.

In the test, the sensor is fixed on the front suspension of a truck with half loads at 50 km/h. Through the test, the motion state of shock absorber can be obtained, and it is presented in Figure 13.

5.2. Optimization and Results. In the optimization, an algorithm named Multi-Island Genetic Algorithm (MIGA) was adopted to perform the process. Considering that the constraint condition should be prioritized, so weight factors of F_{ce} and F_{cy} are 0.5 and 0.5, respectively. The block diagram is shown in Figure 14.

The optimization results are shown in Figure 15. In Figure 15, the relationship between RmsPower and Dis, R is presented. And Table 4 showed the RMS value of energy and the corresponding damping force. After optimization, the regenerated energy increased greatly within the constraint condition. In summary, through an overall consideration, the optimization could improve the performance of HERSA, and it showed the semiactive control of HERSA was feasible.

(a) (b)

(c) (d)

Figure 11: The vehicle test for road roughness. (a) The vehicle in the test; (b) the location of sensor on the shock absorber; (c) the displacement sensor; (d) data collection equipment.

Figure 12: The road surface.

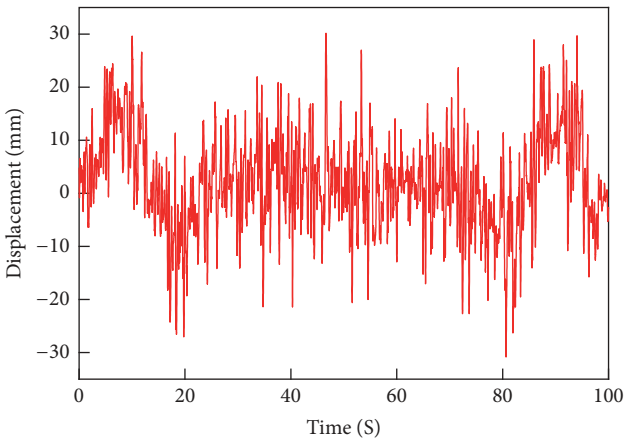

Figure 13: The typical road roughness.

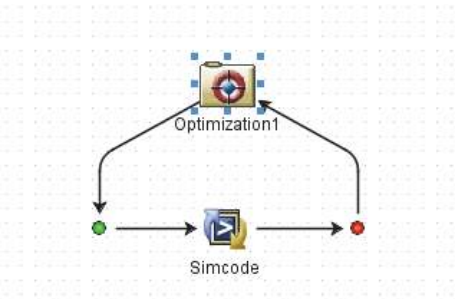

Figure 14: The block diagram in software.

6. Conclusions

This paper presented a novel hydraulic energy-regenerative shock absorber based on the traditional telescopic shock absorber. The design, modeling, and analysis of the HERSA

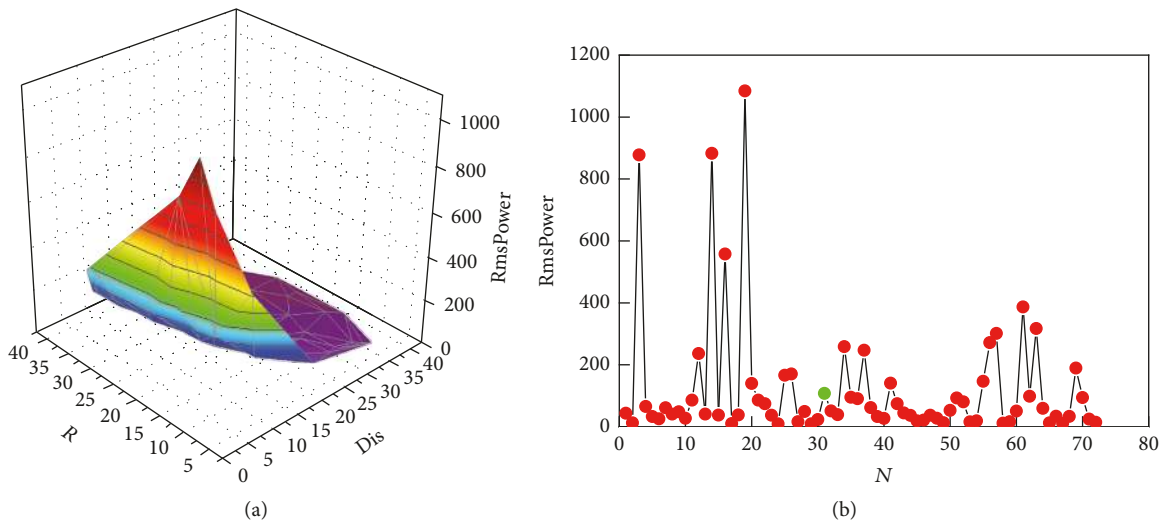

Figure 15: The optimized results. (a) The relationship between RmsPower and Dis, R; (b) the history of optimization.

Table 4: The optimal results.

Variable		RmsPower
Optimal parameter	Dis: 14 R: 18	107.94
Constraint condition	F_{ce}	11298/(N)
	F_{cy}	−5725/(N)

are demonstrated. An accurate mathematical model is proposed based on the hydromechanics theory. The suspension vibration energy is analyzed to evaluate the potential of the power which could be regenerated. In the analysis, the sensitivity of vehicle parameters is researched with the constraints of different road surfaces, and it shows that the tire stiffness had the most influences on the regenerated energy, and it is a positive correlation. Through the theoretical calculation, the maximum energy can be obtained on the road D.

To study the characteristics of HERSA, the parametric analysis of the system is demonstrated in this paper. The crack pressure of check valve, displacement of hydraulic motor, and external load are considered as the variables in the simulation. And the analysis indicated that the displacement of hydraulic motor and external load have large effects on the regenerated energy. To maximize the regenerated energy, an optimization based on the MIGA is carried out. In the optimization process, the displacement data obtained from the road test is regarded as the excitation input in the simulation; the purpose of it is to make the optimization more close to the actual situation. The results indicate that the optimal meets the requirements. In a word, a novel hydraulic energy-regenerative shock absorber was put forward, and the research in this paper could be as a foundation for the late-stage study.

Conflicts of Interest

The authors declare no conflicts of interest.

Authors' Contributions

Junyi Zou and Xuexun Guo contributed mainly to the mechanical sketch design, modeling, and simulation. Lin Xu mainly carried out the data analysis and the paper writing. Gangfeng Tan revised the grammar and the whole paper. Chengcai Zhang offered some useful advice for the research. Jie Zhang offered the design suggestion of the mechanical parts.

Acknowledgments

The authors gratefully acknowledge the National Natural Science Foundation of China (Grant no. 51675391), the Fundamental Research Funds for the Central Universities (Grant no. 155207003), and Wanxiang Group Technology Center.

References

[1] International Energy Outlook, 2016, https://www.eia.gov/outlooks/ieo/.

[2] L. Zuo and X. Tang, "Large-scale vibration energy harvesting," *Journal of Intelligent Material Systems and Structures*, vol. 24, no. 11, pp. 1405–1430, 2013.

[3] Y. Okada and H. Harada, "Active and regenerative control of electro-dynamic vibration damper," in *Proceedings of the Design Engineering Technical Conference*, vol. 3, Part C, pp. 595–602, Boston, Mass, USA, 1995.

[4] Y. Suda and T. Shiiba, "A new hybrid suspension system with active control and energy regeneration," *Vehicle System Dynamics*, vol. 25, supplement 1, pp. 641–654, 1996.

[5] H. Roshani, S. Dessouky, A. Montoya, and A. T. Papagiannakis, "Energy harvesting from asphalt pavement roadways vehicle-induced stresses: a feasibility study," *Applied Energy*, vol. 182, pp. 210–218, 2016.

[6] L. Zuo, B. Scully, J. Shestani, and Y. Zhou, "Design and characterization of an electromagnetic energy harvester for

vehicle suspensions," *Smart Materials and Structures*, vol. 19, no. 4, Article ID 045003, 2010.

[7] Z. Li, L. Zuo, G. Luhrs, L. Lin, and Y.-X. Qin, "Electromagnetic energy-harvesting shock absorbers: design, modeling, and road tests," *IEEE Transactions on Vehicular Technology*, vol. 62, no. 3, pp. 1065–1074, 2013.

[8] S. Singh and N. V. Satpute, "Design and analysis of energy-harvesting shock absorber with electromagnetic and fluid damping," *Journal of Mechanical Science and Technology*, vol. 29, no. 4, pp. 1591–1605, 2015.

[9] X. Tang and L. Zuo, "Vibration energy harvesting from random force and motion excitations," *Smart Materials and Structures*, vol. 21, no. 7, Article ID 075025, 2012.

[10] M. Montazeri-Gh and M. Soleymani, "Investigation of the energy regeneration of active suspension system in hybrid electric vehicles," *IEEE Transactions on Industrial Electronics*, vol. 57, no. 3, pp. 918–925, 2010.

[11] X. D. Xie and Q. Wang, "Energy harvesting from a vehicle suspension system," *Energy*, vol. 86, pp. 385–392, 2015.

[12] R. Wang, F. Gu, R. Cattley, and A. Ball, "Modelling, testing and analysis of a regenerative hydraulic shock absorber system," *Energies*, vol. 9, no. 5, p. 386, 2016.

[13] S. Guo, Y. Liu, L. Xu, X. Guo, and L. Zuo, "Performance evaluation and parameter sensitivity of energy-harvesting shock absorbers on different vehicles," *Vehicle System Dynamics*, vol. 54, no. 7, pp. 918–942, 2016.

[14] R. Galluzzi, A. Tonoli, N. Amati et al., "Regenerative shock absorbers and the role of the motion rectifier," SAE Technical Papers, 2016.

[15] L. Zuo and P.-S. Zhang, "Energy harvesting, ride comfort, and road handling of regenerative vehicle suspensions," *Journal of Vibration and Acoustics, Transactions of the ASME*, vol. 135, no. 1, Article ID 011002, 2013.

[16] Z. Fang, X. Guo, L. Xu, and H. Zhang, "Experimental study of damping and energy regeneration characteristics of a hydraulic electromagnetic shock absorber," *Advances in Mechanical Engineering*, vol. 2013, Article ID 943528, 2013.

[17] Z. Fang, X. Guo, L. Xu, and H. Zhang, "An optimal algorithm for energy recovery of hydraulic electromagnetic energy-regenerative shock absorber," *Applied Mathematics & Information Sciences*, vol. 7, no. 6, pp. 2207–2214, 2013.

[18] A. S. Kammer and N. Olgac, "Delayed-feedback vibration absorbers to enhance energy harvesting," *Journal of Sound and Vibration*, vol. 363, pp. 54–67, 2016.

[19] B. Gong, X. Guo, S. Hu, and Z. Fang, "The ride comfort and energy-regenerative characteristics analysis of hydraulic-electricity energy regenerative suspension," *Journal of Vibroengineering*, vol. 18, no. 3, pp. 1765–1782, 2016.

[20] B. Huang, C.-Y. Hsieh, F. Golnaraghi, and M. Moallem, "A methodology for optimal design of a vehicle suspension system with energy regeneration capability," *Journal of Vibration and Acoustics, Transactions of the ASME*, vol. 137, no. 5, Article ID 051014, 2015.

[21] Z. Fang, X. Guo, and L. Xu, "Energy dissipation and recovery of vehicle shock absorbers," SAE Technical Papers, 2012.